Deployment and Inflation Characteristics Tests of a Buoyant Venus Station Balloon

SY STEINBERG* AND GLENN F. HOLLE†
Martin Marietta Corporation, Denver, Colo.

The Buoyant Venus Station balloon is deployed and inflated during descent under a parachute. Controlled high-volume, low-pressure, diffused flows from high-pressure gas storage are required for rapid inflation of the thin skin balloon. From a group of candidate configurations, a satisfactory diffuser (an overexpanded DeLaval nozzle with a screen cascade to control pressure reduction) was developed experimentally. A cylindrical liner-sock efficiently distributed the subsonic inflation gas within the balloon and transmitted the deployment load to the gondola. Model and full-scale balloons were inflated in quiescent air with helium from 4500-psi, constant-pressure and blow-down sources. Combined deployment and inflation of a 2-mil Mylar balloon was demonstrated in the LRC Full-Scale Wind Tunnel within a sustained environment of greater duration and severity than that anticipated for the Venus atmosphere.

Nomenclature

M = Mach number
P_a = barometric pressure, psia
P_{N_i} = inlet duct pressure at metering nozzle, psia
P_0 = helium recovery duct static pressure, psia
P_s = instrumentation rake static pressure, psia
P_T = instrumentation rake total pressure, psia
q = dynamic pressure, psf
r = radius to instrumentation probe from duct centerline
R = duct radius
T_a = atmospheric temperature, °F
U = velocity, fps
V_b = total (full) balloon volume, ft³
V_i = inflated balloon volume, ft³
β = porosity: pressure reducer porosity is the open flow area divided by the total duct area at the axial location; porous sock porosity is the open flow area divided by total surface area of the sock
τ = time, sec
C = perforated labyrinth cylinder, $\beta = 0.070$
G = screen support grating; $\beta = 0.695$
K = nylon sock cylinder, diameter 7 in.; subscript defines exposed length in ft
L = liner for sock cylinder, 7 in. diam; subscript defines active length in ft
N = metering nozzle; $D_t = 0.151$ in.; $A_t = 0.018$ in.²
P = perforated plate; $\beta = 0.315$
S = pressure reducing screen; subscript defines porosity

Superscript

u = when used with symbol S refers to screen unsupported with Grating G

Subscripts to

S^u,S = numerals refer to fraction of full open screen area
K,L = respectively refers to active exposed length of sock or sock liner

Presented as Paper 69-1017 at the AIAA/ASTM/IES 4th Space Simulation Conference, Los Angeles, Calif., September 8–10, 1969; submitted October 9, 1969; revision received March 2, 1970. Work reported herein supported in part by NASA/LRC Contract NAS1-7590.

* Staff Engineer, Flight Technology Department. Associate Fellow AIAA.
† Senior Engineer, Mechanical Engineering Department.

Introduction

THE concept of a Buoyant Venus Station (BVS)[1] for scientific exploration within the planet atmosphere and on its terrain involves deployment and rapid inflation of a thin-skin superpressure balloon while the BVS descends in Venusian atmosphere suspended on a parachute. The superpressure provides constant balloon volume and consequently flotation at a constant density altitude. The inflating gas is provided from high-pressure storage. Figure 1 illustrates sequential events in BVS deployment, inflation, and establishment. The approximate density altitude is sensed during parachute descent; the chute extracts the balloon from its canister; balloon inflation is initiated and concluded‡; the chute and depleted gas tankage are released; the balloon continues to slowly descend as the environment heats the gas; and the ballon begins to ascend to its buoyant altitude and vent as thermal balance occurs and it reaches the design superpressure volume. The typical altitude trajectory as a function of time to flotation and subsequent surface sonde droppage is also shown in the figure. At time of balloon deployment the descent velocity of about 30 fps exposes the extended balloon surface to a dynamic pressure q of $\sim$1 psf.

Uncertainties in regard to the ability of the balloon to withstand the internal and external flow environments led to an experimental program to demonstrate: 1) a pressure-reducing diffuser system for inflating the balloon so that internal inflation gas dynamic pressure approximately equals the anticipated external freestream q; 2) rapid inflation of a) a representative thin-skin subscale balloon from a constant-pressure (4500 psi) helium gas source in a quiescent external environment using the developed diffuser system, and b) a representative full-scale balloon from a bottled gas source initially pressurized to 4500 psi; 3) the effects of sustained external flow on the deployed full-scale balloon when uninflated and partially inflated in steps; 4) the combined effects of deployment and continuous inflation under simulated external flow conditions and internal mass-flow conditions corresponding to the design criteria.

‡ At inflation conclusion, gas volume of the balloon is $\sim$75% of design super-pressure volume, and the descent velocity is$\sim$ 50% of inflation start velocity.

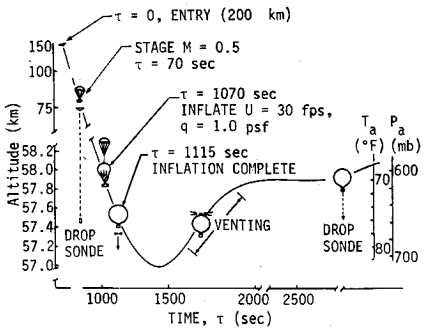

Fig. 1 Entry and deployment sequence.

The following two major sections, respectively, discuss the diffuser development program in combination with the quiescent environment balloon inflations (demonstrations 1 and 2),[2] and the wind-tunnel investigations (demonstrations 3 and 4).[3] The impact of the results and requirements for continued development effort are discussed.

Diffuser Development

Rapid balloon inflation entails high flow rate without violating balloon structural integrity. The metered high-pressure gas must be diffused and subsequently distributed so that high energy flows do not directly impinge upon the internal balloon surface. Large pressure reduction followed by efficient distribution of the gas is required. Pressure reducing devices placed downstream of a metering nozzle or orifice followed by a cylindrical porous sock extending within the balloon and having a diameter approximately equal to the neck diameter of the balloon was conceived as the means to efficiently inflate the balloon. The sock would become a central balloon plenum to evenly distribute high volume gas flows and would also act as a tension member to transfer balloon deployment shock load from the gondola to the parachute, rather than applying this load to the balloon skin.

Schemes for pressure reduction studied analytically included square mesh screens (individually and in a cascade arrangement), a perforated plate with the flow emanating axially, and a perforated cylinder with the flow directed radially. The analytical studies were verified experimentally. Figure 2 shows the test rig assembly, Fig. 3 shows the diffuser configuration components, and Table 1 lists selected pressure reducing device and sock liner material details.

The desired pressure reduction can be obtained by overexpanding the flow (supersonically) and allowing the resultant oblique shock structure to produce the total pressure loss. However, the maximum Mach number during expansion should be limited to avoid condensation. This requires insertion of a physical disturbance to induce shock(s) in the flow upstream from the points at which pressure gradient alone would cause shocks and at which the local flow pressure and temperature would permit condensation. Obstructions induce normal

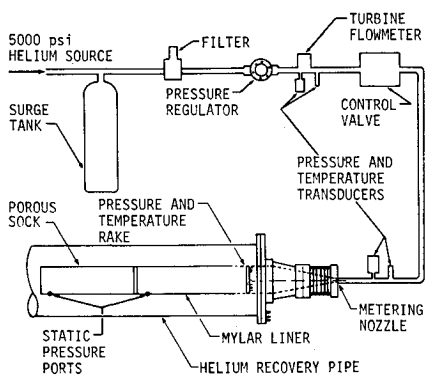

Fig. 2 Diffuser test rig schematic.

Table 1 Pressure reducing devices, physical details

	Diameter, in.	Flow rate lbm/sec
Nozzles/diffuser		
Helium nozzle	0.151	0.72
Nitrogen nozzle	0.406	
Nitrogen orifice	0.344	2.27

Diffuser stations[a]	A	B	C	D	E	F, G
diameter, in.	0.95	1.49	2.02	2.56	3.23	7.0

Screens

Screen mesh	Porosity	Wire diameter, in.	Screen position[a]
5.3[b]	0.695	0.031	
10	0.563	0.025	F and G
16	0.507	0.018	A–E
24	0.307[c]	0.014	
30	0.371	0.013	
50	0.303	0.009	

Perforated obstructions

	Porosity	Material thickness, in.	Number of holes	Hole diameter, in.
Perforated plate	0.315	0.25	323	0.218
Perforated cylinder	0.070	0.25	18	0.218

Cylindrical sock/liner

	Material	Diameter, in.	Length, ft	Porous length of sock, ft
Sock	1.1 oz/yd² nylon (MIL-C-7020D)	7.2	10.4	10.4
Liner	0.5-mil Mylar	7.1	6.9	3.5

[a] Screen locations in the nitrogen diffuser designed for the Langley wind-tunnel test (see Fig. 3).
[b] Screen support grate of 0.25-in.-wide strips of 0.031-in.-thick flat stock.
[c] Porosity of the combined screen and support grate.

shocks, add diffuser drag, and reduce diffuser length, as contrasted to an unobstructed diffuser. An optimum Mach number, at which to shock the flow, may be possible.

The diffuser performance was tested for several configurations: individual screens of three porosities, two- and four-screen cascades, a perforated plate, a perforated cylinder, a labyrinth combination of the perforated cylinder and plate, a diffuser void of mechanical pressure reducing devices, and two configurations of diffuser liner-sock with a selected diffuser design.

Square Mesh Screens and Perforated Plates

The screen must withstand the initial impulse from 4500-psi gas. Accordingly, each screen designed for test was structurally tested initially. The 50-mesh screen failed partially by beginning to shear at the juncture with the diffuser wall and by dimpling of the central area. A central dimple of lesser deformation appeared on the 30-mesh screen, but the 16-mesh screen survived without deformation. In anticipation of possible screen failure, structural support gratings with porosity of 0.695 were fabricated. The grate in combination with a 24-mesh screen provided almost the same porosity as the 50-mesh screen alone.

The distribution of the instrumentation rake total pressure readings across the duct is presented in Fig. 4a for several configurations. Also shown are the wall static pressure data and estimated duct centerline Mach number based on perfect gas, one-dimensional, isentropic flow.

Interestingly, the most even distribution of total pressure for single-screen configurations occurs with the screen of highest porosity. A high-velocity core develops with decreasing

porosity. In fact, a combined screen and support grate configuration porosity of ~31% produced a centerline Mach number ~0.61 at a back pressure of about 28 psia. The effect of reducing back pressure by exhausting to atmosphere rather than into the helium recovery duct was also investigated. The duct centerline Mach number increased to about $M = 1.34$ for the 31% porosity screen configuration at the reduced back pressure. It is possible that shock-induced flow separation was occurring in the nozzle upstream of the screen in both cases. The shock pressure loss coupled with a small pressure loss through the screen is sufficient to cause separation in the boundary layer and to prevent full duct flow expansion downstream of the screen. The core flow characteristics then become a function of back pressure. As back pressure is decreased, the pressure loss in the core is decreased and centerline Mach number is increased. This was perhaps further exemplified by the relative sizes of the screen deformation dimples experienced during the screen structural tests. The screen with porosity $\beta = 0.303$ indicated a high-energy core flow significantly smaller than the duct diameter at the screen station. This was not apparent with the higher porosity screens.

The effect of screen porosity on diffuser exit duct-centerline total pressure, normalized by nozzle inlet static pressure, is presented in Fig. 5. Also shown is the effect on normalized static wall pressure. The effect is quite significant at screen porosities of up to 50%. As porosity was increased to the open diffuser case ($\beta = 1.0$), total and wall static pressures became equivalent within instrumentation accuracy.

For a two-screen cascade system ($\beta = 0.507$), the total pressure distribution across the duct, plotted in Fig. 4a for comparative purposes, was almost constant. The four-screen cascade configuration did not yield noticeably different data from the two-screen cascade.

Two types of perforated plate were tested. One was a cylindrical cap with radial holes that turned the flow by 90° from the axial to the transverse direction. It was reasoned that the 90° change in flow direction provided by the perforated cylinder would eliminate the possibility of establishing a high-energy core flow similar to that shown by the screen configuration in Fig. 4a. The other was a flat plate with the holes in the flow direction. The total pressure distribution across the duct at the survey rake for both configurations is plotted in Fig. 4a and shows the distributions to be nearly constant.

Empty Diffuser

Tests with the diffuser without pressure reducing devices were made. With a 28 psia back pressure, the rake pressure ratio (P_s/P_T) was approximately unity at all reservoir pressures. Figure 4b shows the pressure ratio distribution across the duct for a back pressure reduction of 17 psi at a nozzle inlet pressure of ~4600 psia. The Mach number gradient across the duct was negligible at 28.7 psia back pressure, but became sizeable when back pressure was reduced to 11.9 psia (see Fig. 4b). Also, the open diffuser configuration produced unsteady flow with centerline total pressure fluctuations at a peak value of ~25% of the steady-state value.

The sensitivity exhibited by the empty diffuser is not apparent for the case where mechanical pressure reduction means are employed, as exemplified by the two-screen cascade in Fig. 4b for the same back pressure reduction. Flow instability did not occur with the screen cascade configuration or the perforated plates.

Liner-Porous Sock

The liner-porous sock configuration provides several functions: an internal plenum chamber for the balloon; channels the gas to the balloon crown for progressive inflation from crown to inlet; distributes the inflating gas evenly within the balloon thereby providing local protection for the balloon skin; and absorbs balloon deployment shock loads.

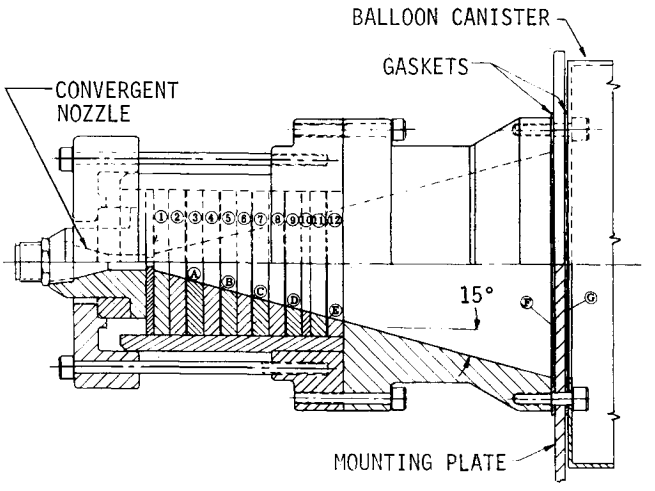

Fig. 3 Diffuser configuration details.

A cylindrical geometry was chosen for the diffuser sock because of simplified fabrication and axial load transfer characteristics. The diffuser sock material porosity requirement was based on the assumptions that the total pressure loss along the sock is negligible, and static pressure down the inside wall may be considered constant for very low Mach number (axial) flow.

Two configurations were run: a no-liner, long porous sock configuration; and a long-liner, short porous sock configuration. The pressure differential across the sock was measured near the sock inlet and at the extreme end of the sock (see Fig. 2). In the long sock case the upstream sock transducer

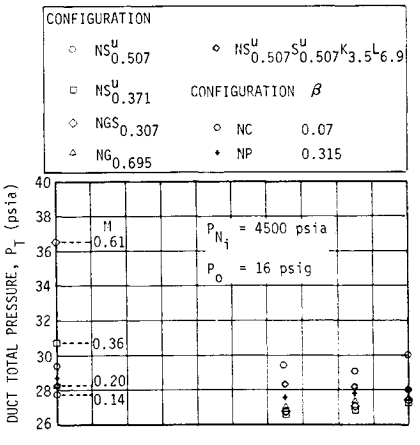

Fig. 4a Distribution of rake total pressure measurements for screen and perforated plate configurations.

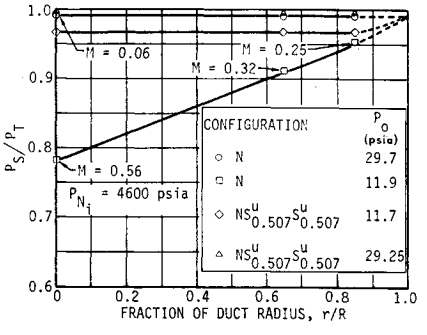

Fig. 4b Distribution of rake static to total pressure ratio for the empty diffuser and a cascade screen configuration.

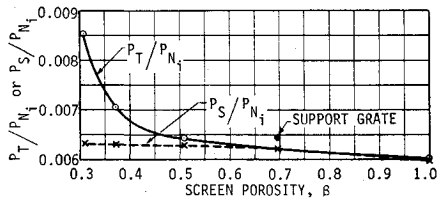

Fig. 5 Effect of screen porosity on diffuser exit duct centerline total and static pressure ratio.

indicated that gas was being pulled from outside the sock to within. The crown transducer, of course, indicated gas leaving the sock. In the long-liner, short sock arrangement, both transducers indicated higher pressure within the sock than outside. In all cases the pressure difference was ~0.1 psi. The latter configuration was selected for subsequent balloon inflation checks.

Analytical vs Experimental Results

An analytical model was developed in an effort to predict diffuser performance with various pressure reducing devices. The model was based on perfect gas, one-dimensional, isentropic relationships and included empirical data.[4] The model was used to design the diffuser configurations, but the separation phenomena that occurred under certain conditions were not predicted.

Quiescent Balloon Inflations

The rapid inflation of a subscale balloon and a full-scale balloon, both of thin-skin construction, was demonstrated under quiescent ambient conditions. Table 2 lists balloon characteristics. On the basis of the diffuser performance tests, a two-screen cascade system was chosen for the rapid balloon inflation checks.

The subscale balloon inflations employed the regulated, constant-pressure helium supply utilized during diffuser development. Two inflations were performed with the smaller balloon: one at a nozzle inlet pressure of 2500 psi (~15 sec in duration) and one at 4500 psi (concluded after 8 sec). Both inflations were to ~90% of available balloon volume.

The high-pressure gas storage onboard the BVS was simulated for the full-scale balloon inflation by manifolding five high-pressure gas storage bottles containing approximately 2400 std ft³ of helium pressurized to 4500 psi. During the ensuing balloon inflation the system blew down to 150 psig in 60 sec. Both quiescent inflation tests were performed successfully without difficulty or hardware damage.

Wind-Tunnel Investigations

The influence of external flow during the deployment/inflation process was determined by two tests of the balloon subsystem in a simulated entry environment at the NASA-Langley Research Center Full-Scale Wind Tunnel.[5] Figure 6 is an exploded pictorial of the BVS model used for these tests. Figure 7 shows the BVS model, high-pressure nitrogen inflation system and instrumentation. A full-scale representation of the gondola and high-pressure gas tankage, the balloon subsystem, and a "battleship" throttling nozzle-diffuser comprise the model.

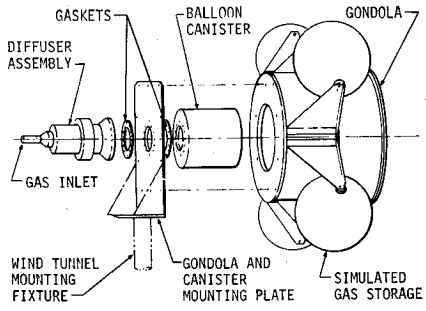

Fig. 6 Exploded pictorial of model components.

Table 2 Balloon characteristics[a]

Type	Subscale cylindrical zero pressure	Full-scale spherical super pressure
Diameter, ft	8.0	16.4
Height, ft	23.0	19.0
Volume, ft³	775.0	2312.0
Material, Mylar laminate, mil	½ × ½	¾ × ½ × ¾
Sock		
Diameter, in.	7.0	13.0
Length, ft	10.4	12.0
Material, oz/yd²	1.1 oz nylon	1.25 oz Dacron
Sock-liner		
Diameter, in.	7.0	13.0
Length, ft	6.9	8.0
Material, Mylar, mil	½	¾ × ½ × ¾

[a] Balloons were supplied by Raven Industries Inc., Sioux Fall, S.D. All materials and construction conformed to standard practices.

Since the model had to be oriented horizontally for testing in the tunnel, an inert, neutrally buoyant inflation gas was desired. Nitrogen gas regulated to 1500 psi from a facility supply was available in the tunnel. The inflation system diffuser configuration used in this investigation (details sketched in Fig. 3) was a modification of the diffuser used in the diffuser development and static inflation tests. At the diffuser/adapter can junction, in the subsonic section, a two-layer screen section was added to ensure complete degradation of total pressure. An average inflation rate of 1185 std ft³/min of nitrogen was achieved from a balloon inlet total pressure of 1100 psi.

The first test was initiated with the uninflated balloon deployed in a 1 psf dynamic pressure airstream, corresponding to a velocity of ~30 fps. The balloon was inflated in steps to 13, 25, and 38% volume so that balloon dynamics could be correlated with balloon geometry.

The second test was to determine the effect of the free-stream on deployment and inflation. The uninflated balloon was folded and packed in the gondola. A polyethylene cover was placed over the open end. Approximately 60 ft of bungee cord under 35 lb of tension was used to provide a nearly constant extraction force over the 20 ft of free travel. The cover was pulled free before the balloon was deployed. The tunnel was stabilized at a dynamic pressure of 1 psf and the balloon was deployed and inflated to 42% volume. The test showed that the air stream had little effect on the balloon deployment or the uninflated balloon. The gondola generated very little unsteady wake at a 30 fps velocity so that the limp balloon skin exhibited only minimal local skin flutter.

Gas entered the balloon uniformly through the diffuser sock. At the first signs of balloon expansion, the external air-

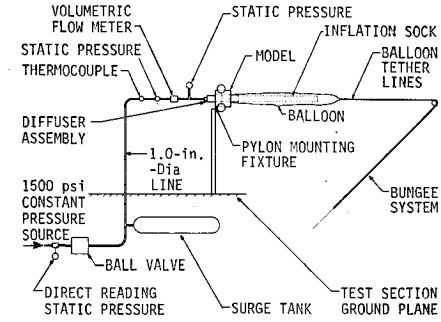

Fig. 7 General arrangement of BVS model in the full-scale tunnel.

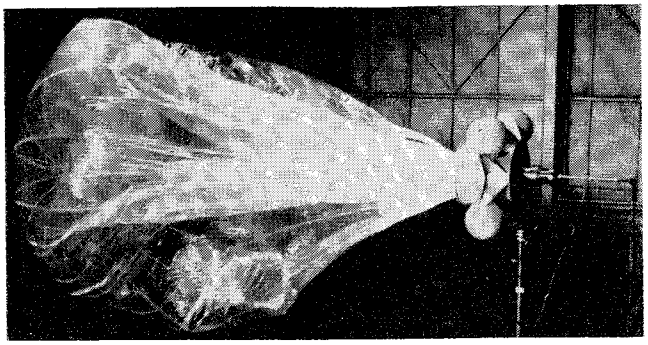

Fig. 8 Balloon inflation during test.

flow forced the inflation gas into a bubble that traveled to the crown.§ Balloon skin flutter became more pronounced in the transition region to the bubble. At this point the unsteady wake from the bubble generated lateral oscillations. As bubble size increased, the flow field interacted with the bubble to produce low frequency longitudinal oscillations. During a longitudinal oscillation, a volume of gas appears to be moved from the bubble toward the neck of the balloon. Interactions between external flow, balloon skin stress distribution, and the inflation gas appear to determine the amplitude of the motion, which is limited by the length of uninflated balloon. As the moving volume of gas dissipates, its direction reverses, and it returns to the bubble to complete a type of breathing motion. As inflation proceeds with an attendant increase in bubble diameter, the amplitude of both the transverse and longitudinal modes of oscillation increased. It was also noted that the oscillation amplitude was considerably reduced during the inflation process over that experienced during the first test when inflation took place in steps and the dynamics were observed at the specific fixed gas volumes at steady-state. Figure 8 is a photograph of the balloon inflating in the 30 fps airstream. Figure 9 is a photograph of the same balloon after inflation and without external airflow. Lateral motion is restrained by the tether simulating the parachute load. As balloon motion increases, the crown described a circular motion about the centerline.

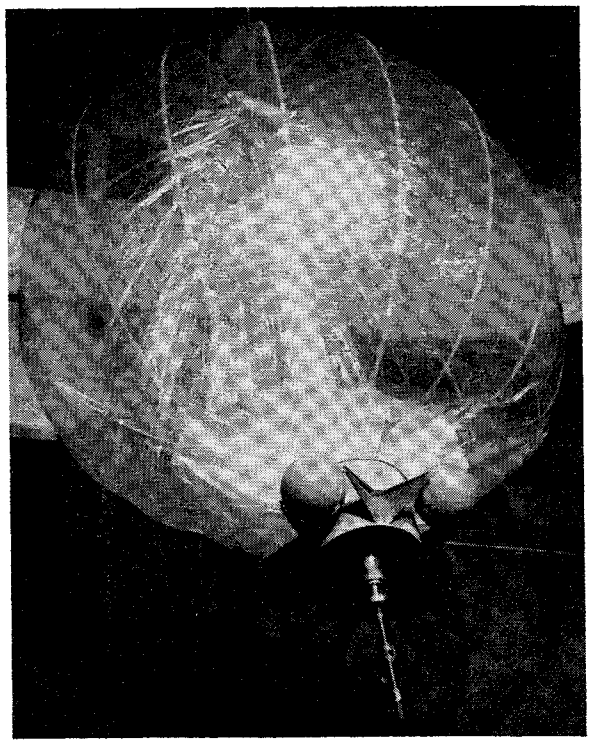

Fig. 9 Balloon in quiescent environment after test.

§ In a quiescent environment, rapid balloon inflation with a buoyant gas also produces a bubble in the balloon crown.[2] Inflation proceeds from the top of the balloon to the bottom.

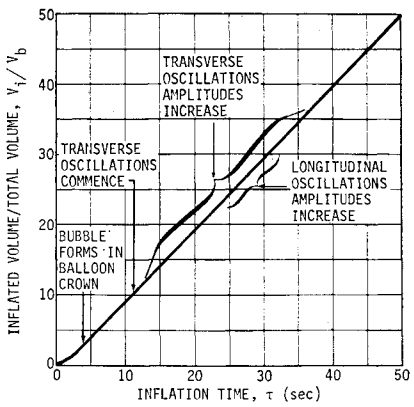

Fig. 10 Typical balloon inflation sequence in 30 fps airstream at the Full-Scale Tunnel.

Motion pictures indicated that the onset and strength of both the transverse and longitudinal oscillations are approximately repeatable, although they are randomly distributed. Visual data on the dynamics of the 16.4-ft-diam balloon could be correlated grossly into the curve shown in Fig. 10. It is probable that these data apply only to the nitrogen inflation system used in the wind tunnel since the lighter inflation gas to be used in the BVS would react differently with the external flow environment, being predominantly influenced by the diminishing total pressure in a blowdown system. No structural damage to the balloon was sustained due to deployment or inflation dynamics associated with the properly simulated model loads.

Conclusions and Recommendations

Based on the data obtained during the diffuser evaluation tests, the following conclusions were reached:

1) Square mesh screens of greater than 50% porosity are adequate for reducing total pressure of a gas for inflating thin skin balloons. At lower porosity a high-energy flow forms on the duct centerline, probably as a result of flow separation upstream of the screen.

2) A perforated plate with longitudinal or transverse hole configurations provided a steady, well-diffused flow. However, the hardware is very heavy.

3) A diffuser without pressure reducing devices is potentially usable, but sensitive to back pressure. This suggests that the pressure reducing process in the diffuser requires considerable length. This type of diffuser also appears conducive to unsteady and unstable flows. Peak-to-peak pressure fluctuations of about 25% of the absolute pressure value were experienced.

4) A two- or four-screen cascade system yielded good results in that low subsonic flow and constant total pressure occurred across the 7-in.-diam duct. The flow was smooth and steady.

5) A long-liner coupled with a short porous sock appears to be a desirable central balloon plenum and gas distributing device.

6) A thin-skin superpressure balloon of capacity equivalent to a 11.4-ft-diam spherical balloon may be inflated in 7 to 8 sec from a 4500 psi constant pressure helium source under quiescent conditions.

7) A 16.4-ft-diam balloon can be inflated from 4500 psi helium storage of 7.5 ft^3, blown down in 60 sec.

The motion pictures obtained during the wind-tunnel tests show that:

1) A balloon constructed from commercially available Mylar film using present balloon manufacturing practices can be successfully inflated under BVS dynamic conditions.

2) A balloon can withstand the combined effects of internal and external flows, both individually and collectively, without any evident damage in a sustained environment of greater

duration and severity than would be encountered within the Venus atmosphere.

3) The amplitude of lateral and longitudinal oscillations of a tethered balloon is a direct function of the volume of gas within the balloon; the balloon oscillations appear to be less pronounced while inflation is taking place as contrasted to those experienced in a steady-state condition of specific volumes without gas entering the balloon.

4) The longitudinal oscillations of the balloon have a frequency of about $\frac{1}{2}$ cps at maximum amplitude. The lateral oscillations include a rolling moment, and with the tether taut, the balloon end cap describes a circular motion about the longitudinal centerline of the balloon.

For additional development the initial component developments and system feasibility demonstrations described herein should be followed by additional system functional tests, a comprehensive materials study for selection of an appropriate sterilizable balloon material, and a flight demonstration of the complete BVS under simulated conditions in the Earth's atmosphere.

References

[1] Carrol, P. C., Frank, R. E., and Pettus, J. D., "Buoyant Venus Station Mission Feasibility Study for 1972–1973 Launch Opportunities," NASA CR-66725-3, Jan. 1969, Martin Marietta Corp., Denver, Col.

[2] Steinberg, S. and Holle, G. F., "Experimental Results of a Diffuser Configuration Designed for Rapid Inflation of a Superpressure Balloon," FTD Report 0473-68-01, June 1968, Martin Marietta Corp., Denver, Colo.

[3] Holle, G. F., Steinberg, S., and Carroll, P. L., "Wind Tunnel Test Results of the Deployment/Inflation Characteristics of a Model Balloon (Buoyant Venus Station Concept)," MCR-69-23, Jan. 1969, Martin Marietta Corp., Denver, Colo.

[4] *Royal Aeronautical Society Data Sheets*, Vol. 5, Issue 15, No. 02.00.01–02.00.02, 1964.

[5] Steinberg, S., "Pretest Report and Test Plan for a Preliminary BVS Balloon Wind Tunnel Test," MCR-68-456, Nov. 1968, Martin Marietta Corp., Denver, Colo.

JULY 1970 J. SPACECRAFT VOL. 7, NO. 7

Longitudinal Temperature Profiles in Fluid Flow and Considerations in Thermal Modelling

THEODORE C. YORK*
Toronto, Canada

A method for the inclusion of fluid flow phenomena in a heat-transfer computer program has been developed that relieves the difficulties presently experienced with stringent stability criteria. These difficulties are because of the assumption that T_{av}, the average between inlet and outlet temperatures, can always be used as bulk temperature (T_b). This assumption has been made to remedy the condition of two unknowns, T_b and the outlet temperature (T_0), whereas there is only one equation for the heat balance in a fluid nodal volume. The change in T_0 can always be derived from heat-transfer relationships, thus eliminating one of the two unknowns. The other unknown, T_b, can be computed correctly from the energy balance. Hence the various components that contribute to the energy balance in a fluid volume are separated and can be dealt with individually, whereas previously they were obscured by the assumption that $T_b = T_{av}$. Only when there is a full gradient through the node does $T_b = T_{av}$. Some restrictions that still exist because of the linear assumptions of the method are pointed out.

Nomenclature†

CAP = thermal capacitance of fluid node, Btu/°F Fortran notation is used for clarity
c_p = specific heat of fluid, Btu/(°F − lb)
h_c = convective heat transfer coefficient, Btu/(hr − °F − ft²)
L = length of nodal volume, ft
P = perimeter of enclosure, ft
$\dot{q}$ = rate of heat flow to fluid, Btu/hr
Δt_H = hydraulic time step defined in text
Δt_t = time step dictated by thermal system
T = temperature, °F; $T_{av} = (T_i + T_0)/2$
ΔT = $T_i - T_0$
$\dot{w}$ = flow rate of fluid, lb/hr

Subscripts

b = bulk
i,o = inlet and outlet of node, respectively
w = at wall

Presented as Paper 69–30 at the AIAA 7th Aerospace Sciences Meeting, New York, January 20–22, 1969; submitted April 3, 1969; revision received February 11, 1970. Most of the work described in this paper was performed during employment with McDonnell Douglas Astronautics Company, Huntington Beach, Calif. The author would like to thank W. P. Sokeland, also formerly with McDonnell Douglas Astronautics Company, for his suggestions and contributions in support of this work.

* Consulting Engineer.

† Unprimed quantities are the properties at the beginning of a time step. Primed quantities are the forward properties at the end of a time step.

Introduction

CLASSICAL textbooks on heat transfer, while exploring the evaluation of convective heat-transfer coefficients to great depth, give little information on how to evaluate temperatures in the fluid numerically. The advent of computers led to the advancement of numerical techniques. Several methods were developed for evaluating the Fourier and the Laplace equations. They are used in the many heat-transfer programs existing throughout the industry and con-